

Original Article

Chondrogenesis in primitive tracheal neocartilage: insights from 3D-printed silicone grafts in a large-scale animal model

Sen-Ei Shai^{1,2,3*}, Yi-Ling Lai^{1*}, Yi-Wen Hung⁴, Chi-Wei Hsieh⁵, Kuo-Chih Su⁶, Chun-Hsiang Wang⁶, Te-Hsin Chao⁷, Yung-Tsung Chiu⁸, Chia-Ching Wu^{5,9}, Shih-Chieh Hung^{10,11}

¹Division of Thoracic Surgery, Taichung Veterans General Hospital, Taichung 407219, Taiwan; ²Department of Applied Chemistry, National Chi Nan University, Nantou 545301, Taiwan; ³Institute of Clinical Medicine, National Yang-Ming Chiao-Tung University, Taipei 112304, Taiwan; ⁴Terry Fox Cancer Research Laboratory, Translational Medicine Research Center, China Medical University Hospital, Taichung 404327, Taiwan; ⁵School of Medicine, National Cheng Kung University, Tainan 701401, Taiwan; ⁶Department of Medical Research, Three Dimensional Printing Research and Development Group, Taichung Veterans General Hospital, Taichung 407219, Taiwan; ⁷Division of Colon and Rectal Surgery, Department of Surgery, Chiayi and Wanggiao Branch, Taichung Veterans General Hospital, Chiayi 600573, Taiwan; ⁸Department of Medical Research and Education, Taichung Veterans General Hospital, Taichung 407219, Taiwan; ⁹Department of Cell Biology and Anatomy, College of Medicine, National Cheng Kung University, Tainan 701401, Taiwan; ¹⁰Integrative Stem Cell Center, China Medical University Hospital, Taichung 404327, Taiwan; ¹¹Institute of New Drug Development, China Medical University, Taichung 404328, Taiwan. *Equal contributors.

Received September 23, 2024; Accepted January 18, 2025; Epub February 15, 2025; Published February 28, 2025

Abstract: Objectives: Tracheal cartilage has limited regenerative potential in adults, posing a significant challenge for tracheal repair. Here, we observed marked neocartilage growth in a porcine model after transplanting it with a three-dimensional (3D)-printed silicone tracheal graft. Methods: Virtual silicone tracheal grafts of 2 cm in length were first generated using a 3D printer, and simulated a 3-month-old porcine trachea based on data from physical stress tests. After a segmental resection, a graft underwent end-to-end anastomosis at both the proximal and distal tracheal sections. Neotissue samples were later examined macroscopically, and their histologic properties were assessed based on results from the following: protein expression using H&E staining, alcian blue and safranin O/fast green staining for glycosaminoglycans (GAGs), and immunohistochemistry (IHC) assays for Sox9, type II collagen, aggrecan, and proliferating cell nuclear antigen (PCNA). Results: These primitive cartilages displayed chondrogenesis with an initial surplus of chondrocytes, evolving into a mature, stable state with cartilage corrosion facilitated by interim perichondrium-derived chondro-modulators, like perichondrial papillae (PPs), preresorptive layers (PRLs), and vascular canals (VCs). Results of alcian blue staining revealed the removal of matrix degradation products, specifically in the vicinity of the mucosal and submucosal glands. Conclusions: Chondrogenesis underwent an initial burst of growth together with the perichondrium, constituting a gradual consolidation process. Such a consolidation was supported by the emission of matrix degradation products in the mucosa and submucosa. To summarize our results, we propose a four-stage scheme to characterize the regenerative chondrogenesis of tracheal neocartilage.

Keywords: Primitive tracheal neocartilage, large-scale porcine, chondro-modulators, perichondrium, de novo cartilage growth

Introduction

In adults, the regenerative potential of tracheal cartilage is very limited, making cartilage repair highly challenging. Regarding tracheal transplantation, experimental studies reported rath-

er sporadic successes, with no consensus on the best material or method. Approaches in transplantation include the following: allograft, autograft, prosthetic, autologous tissue-engineered trachea, nano-composite of tracheal biomaterial with stem cell seeding, and decel-

ularized donor trachea [1-7]. While significant progress has been made in understanding the general mechanisms of tissue regeneration, the specific nuances of tracheal regeneration remain a subject of ongoing investigation. Despite recent strides in understanding tracheal regeneration, a research gap exists regarding the precise stages of chondrogenesis and modulating factors influencing the outcome.

One potential source for cartilage regeneration is the perichondrium [8, 9]. Cartilage homeostasis involves various growth factors and signal transductions, with the exact nature of this complex process unclear [10]. In 2017, Gabner et al. working on the nose and rib cartilages of newborn piglets, discovered vascular canals (VCs), revealing their relevance to this homeostasis process [11]. In our previous study, we reported the *de novo* generation of cartilage within three-dimensional (3D)-printed grafts related to the maturation of chondrocytes in terms of their numbers [12]. These grafts driven neocartilage contain chondro-modulators, such as perichondrial papillae (PPs), preresorptive layers (PRLs), and VCs. Although the requirements for chondrogenesis are understood, the process from initial budding to maturity has been less explored. Regenerative medicine in large animals offers superior conditions for observing regenerative development compared to embryonic studies. We have analyzed the newly regenerated cartilage using 3D tracheal grafts in an attempt to establish a mechanism for chondrogenesis.

Our study aims to bridge this research gap by providing a detailed account of the sequential stages of chondrogenesis during tracheal regeneration. Advanced 3D printing technology holds promise for customizing objects with a shape compatible with a functional trachea for clinical application [13, 14]. Additionally, large-scale animal models can accurately reflect clinical applications in humans, making preclinical animal trials for tracheal transplantation critically important, despite the small sample size and challenges in postoperative care and monitoring [15]. The prevailing hypothesis on tissue regeneration is that this 3D printing approach, using an organism as an optimal bioreactor, promotes progenitor or stem cell homing, resulting in the *de novo* regeneration of tracheal cartilage.

Materials and methods

Participants

Male LY pigs (n=10) were acquired from a commercial source, Pinguan Modern Livestock Co., Ltd., Taichung, Taiwan. Animals were ~three months old, with body weights ranging from 25 to 40 kg. Our study was approved by the Institutional Experimentation Committee of Taichung Veterans General Hospital (Animal Welfare Protocol Number La-1101785, approved May 11, 2021). A total of 10 pigs were initially included in the study, but seven were later excluded due to following reasons: undetected cartilage regeneration (one animal), wound infections (two animals), and unexpected deaths (four animals). Finally, a total of three remaining animals were examined, producing 16 tissue specimens. In addition, two native tracheal tissue specimens were obtained each from three- and six-month-old pigs for comparison of chondrogenesis study (**Figure 1**).

Graft design and preparation

We employed simulated tracheal implants constructed from silicone material. Silicone implants are widely used in tracheal stents due to their non-toxicity, inertness within the body, and ease of surgical anastomosis. These implants ensure an air-tight fit while maintaining good elasticity, enabling the graft to provide structural support and prevent tracheal collapse after transplantation.

Using SolidWorks software, we specifically designed and manufactured silicone tracheal grafts for large porcine tracheal transplantation. The S050 silicone 3D printer (San Draw Inc., USA) was used to fabricate the grafts, with dimensions of 20 mm in length, 20 mm in diameter, thickness of 1.5 mm and 90% infill. Medical-grade silicone (SIL28, San Draw Inc., USA) was used, with the material extruded and cured layer by layer at a thickness of 2.0 mm per layer to form the tracheal graft. The entire fabrication process required 3-4 hours to complete [15]. The graft resilience was determined using the JSV-H1000 instrument (Japan Instrumentation System Co., Nara, Japan), confirming that these grafts exhibited physical stress properties similar to the native trachea of a three-month-old pig. Before transplantation, these grafts were surface-polished before

3D-printed silicone grafts in animal model

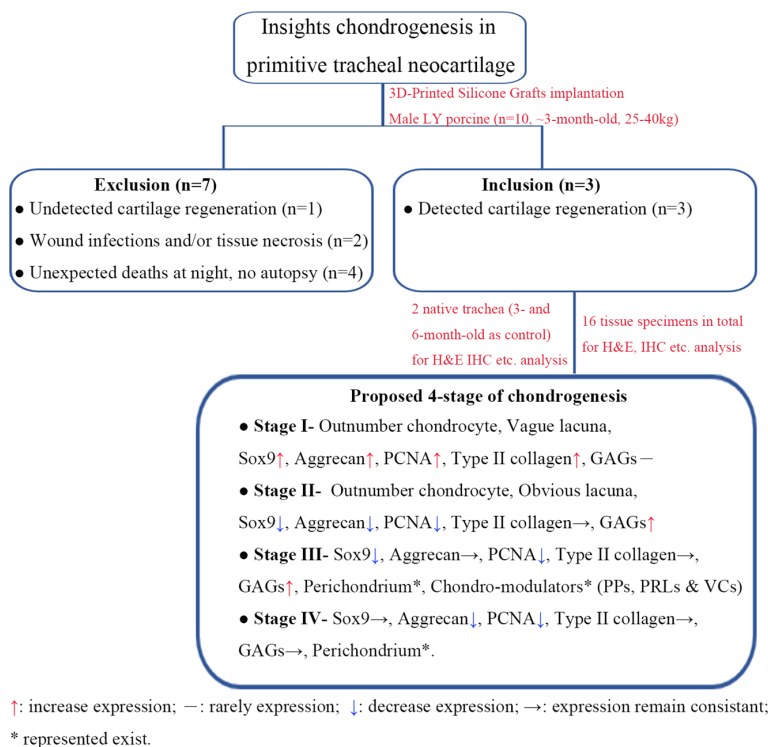


Figure 1. Schema of chondrogenesis in primitive tracheal neocartilage.

sterilized in an autoclave. Aseptic 3D-printed grafts in their best condition were selected as implants.

Surgical intervention

Each pig underwent general anesthesia. The induction was by Zoletil 50 (8 mg/kg, IM, Virbac, Carros, France), followed by intubation using an endotracheal tube of 7.0 mm in diameter. Anesthesia level was maintained using 4% isoflurane. The experimental animal was placed in a supine position, with neck skin shaved and sterilized with povidone iodine and 75% alcohol. The skin area was then draped within a disposable sterile towel. A cervical six cm midline incision was made, and the wound deepened with underlying strap muscles separated to expose the upper trachea. After mobilization of the trachea, a two cm long tracheal segment just below the larynx was marked, surgically removed, and then replaced by a 3D-printed tracheal graft (Figure S1). The procedure involved a segmental resection on a two cm circumferential tracheal segment, followed by an end-to-end anastomosis with the proximal and distal parts of the trachea using non-absorbable sutures (Video S1, Procedures of surgical intervention of Silicone tracheal graft). This

emulated the human virtual operation. Cross-table ventilation was applied during the creation of the anastomosis at the proximal end. The same procedure of anastomosis was applied to both the proximal and distal sections. The proximal trachea was connected with the graft using a 3-0 prolene posterior end running suture and a 4-0 prolene anterior end interrupt suture. After completing the lower posterior half of the distal trachea with graft anastomosis using a 3-0 prolene continuous running suture, the endotracheal tube was re-advanced through the tracheal graft into the distal trachea. The anterior half of the distal trachea was then anastomosed using a 4-0 prolene interrupted suture placed above the endotracheal tube. Lastly, a tracheal bilateral

traction suture was applied at both the proximal and distal ends, tying together each side to relieve tension over the anastomosis. An airtight seal was finally confirmed before closing the strap muscles. A silicone Penrose drain was placed, and the wound closed in layers. Animals were extubated immediately in the operating room after the end of anesthesia. These animals all recovered without complications, resuming normal activities and oral food intake within 12 hours.

Postoperative care

Postoperative medications included pain reliever (diclofenac potassium, 25 mg), antibiotics (ampicillin, 500 mg), and mucolytic solution (bromhexine hydrochloride, 2 mg/ml) (Table S1). They were administered by mixing with food. All animals were managed and cared for by the veterinary team. Feeding procedures were in compliance with both national and international guidelines.

Tissue analyzed with H&E and specific stains

Following an animal's death, an autopsy was performed to harvest graft-related tissues. Tissue samples, fixed in 10% formalin before

3D-printed silicone grafts in animal model

embedded in paraffin, were examined grossly. Histological staining for glycosaminoglycans (GAGs) included H&E, alcian blue (ScyTek, ANC250), and safranin O/fast green (Cat. #8348a/Cat. #8348b). The staining process has been detailed in Shai et al., 2021 [16]. Photomicrographs were taken with the NDP.view 2.6.8 software. Chondrocyte numbers were determined from H&E-stained sections using ImageJ 2 software, and neocartilage matrix contents (glycosaminoglycans, GAGs) were assessed from sections stained with alcian blue and safranin O/fast green. Total pixel areas within sections of H&E-stained cartilage were quantified according to distinct lacunar morphological features. Results were compared between neocartilage and native tracheal cartilage (as from experimental subjects and a 6-month-old mature porcine with stationary tracheal cartilage, Stage IV).

Chondrogenesis detected by Immunohistochemistry (IHC)

Sections were successfully stained with chondrocyte markers, including Sox9 (Biorbyt, orb4387), type II collagen (Abcam, ab34712), and aggrecan (Biorbyt, orb10066). Proliferating cells were detected using the proliferating cell nuclear antigen (PCNA, Abcam, ab29) assay. Angiogenesis in neocartilage was assessed with CD31 (Abcam, ab28364), a blood vessel marker, and quantified using the UltraVision LP Detection System HRP Polymer & DAB Plus Chromogen (Thermo, TL-060-HD, Thermo Fisher Scientific Inc., Waltham, MA USA). Photomicrographs were captured using the software NDP.view 2.6.8. Using Image J software, summed pixel areas were calculated in cartilage sections containing positively IHC stained chondrocytes (against Sox9, aggrecan, and PCNA) [16].

Statistical analyses

Images taken from each slide were randomly reviewed and analyzed by an individual with no prior knowledge of the study. Data were presented as mean \pm SD and compared statistically using the Kruskal Wallis/ANOVA test. Numbers of chondrocytes in the cartilage across different tissues were compared using the Dunn-Bonferroni test/Bonferroni test. Statistical significance was set at $P < 0.05$. Using Image J software, we calculated the num-

ber of chondrocytes in H&E-stained sections and the number of chondrocytes expressing various proteins (Sox9, aggrecan, and PCNA) for each stage ($n=4$ for each group).

Results

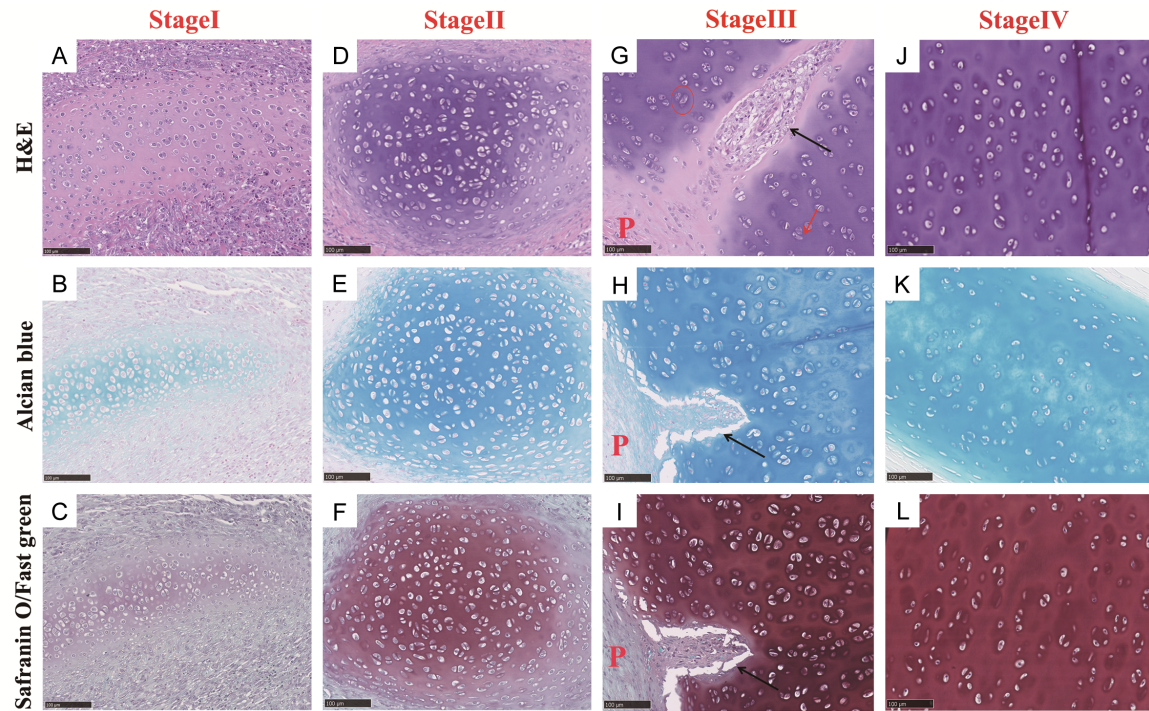
Neotissue outside of tracheal graft with cartilage, muscle, adipose tissue, and glands

We observed vivid neo-tissue growth, encompassing cartilage, muscle, adipose tissue, and glands, in areas outside the 3D-printed tracheal graft (Figure S2). Notably, the integral cartilage regenerated markedly and ectopically early within ~5 days. The chondrogenesis observed in the regenerated tracheal cartilage of large-scale porcine mirrors the process of embryo development. During this stage of regeneration, chondrogenesis occurs in the patterns of apposition and intussusception. The fundamental process of neocartilage growth appears either as an elongation followed by concomitant expansion, or eventually fuses at both ends, forming a single structure (Figure S3A-D). For control study, through the native trachea of the 3-month-old pig, we also observed a horizontal elliptical shape of the tracheal lumen (Figure S4A, S4C), which was noted with a nearly vertical elliptical shape by 6 months (Figure S4B, S4D). It is worth pointing out that tracheal cartilage, distinct from articular cartilage, relies on the presence of the perichondrium for maturation. The perichondrium provides essential nutrients, enabling metabolic processes within the inner core of the cartilage. Following transplantation, the initial area of neocartilage lacks the perichondrial coverage. The perichondrium gradually develops along the edge of the growing cartilage (Figure S3E-H). We classified the transitional stages of developing consolidated cartilage into 4 distinct stages based on the observed histologic patterns (Figure S3I-P).

Dynamic progression of chondrocyte activity and perichondrium formation in neocartilage development

Cartilage development in neotissue: H&E and special stains: In the early stages of cartilage development, neotissue undergoes transitional phases marked by a burst of growth and the formation of numerous unorganized chondrocytes, which create ectopic cartilage islands or

3D-printed silicone grafts in animal model



M

Structures	Stage I (n=4)		Stage II (n=4)		Stage III (n=4)		Stage IV (n=4)		p value
	mean	±SD	mean	±SD	mean	±SD	mean	±SD	
Chondrocytes	173.25	±14.31	115.50	±7.55	53.75	±5.32	51.00	±1.41	0.001**
Perichondrium	No		No		Yes		Yes		
VCs, PPs & PRLs (interim)	No		No		Yes		No		
Protein expression									
Alcian blue	++		+++		++++		++++		
Safranin O/ fast green	+		++		++++		++++		

Figure 2. Proposed stages of chondrogenesis within the graft neo-tissue as seen through H&E, alcian blue, and safranin O/fast green stains: A, D, G, J. The histology of different stages of cartilage during chondrogenesis as investigated with H&E staining. Red circles mark an isogenous group of chondrocytes; red arrows mark a territorial matrix of chondrocytes. B, E, H, K. The histology and GAG content of the different stages of cartilage during chondrogenesis as investigated with the alcian blue staining. GAGs of the cartilage matrix were detected by alcian blue and marked in blue color. C, F, I, L. The histology and GAG content of the different stages of cartilage during chondrogenesis as investigated with safranin O/fast green staining. GAGs of cartilage matrix were detected with safranin O/fast green, as marked in red color. Red “P”: the perichondrium. Black arrows mark the modulator structure of the perichondral papillae (PP). Images were at 200x magnification. M. Quantitative analysis of chondrocyte numbers and structural features across different stages. Statistical significance is denoted by $P < 0.05$. “No” indicates absence, and “Yes” indicates presence. Staining intensity is represented for Alcian blue and Safranin O/fast green using a relative scale: + indicates weak staining; ++ indicates moderate staining; +++ indicates strong staining; ++++ indicates very strong staining.

templates. These early cartilages lack defined lacuna, and the extracellular matrix remains underdeveloped (Figure 2A), as indicated by minimal GAG staining (Figure 2B, 2C). As development progresses, the morphology of chondrocytes evolves, with clear lacunae forming and a reduction in chondrocyte numbers

(Figure 2D). Positive GAG staining highlights the gradual accumulation of the extracellular matrix (Figure 2E, 2F). By stage III, distinct chondrocyte groups (isogenous groups) are identifiable within a loosely arranged regional matrix (territorial matrix) (Figure 2G). Neo-cartilage at this stage exhibits higher levels of

GAG compared to earlier stages, along with the presence of chondro-modulators such as PP, PRL, and VC (**Figure 2H, 2I**). These regulatory structures, originating from the perichondrium, play a key role in cartilage development by modulating chondrocyte activity and numbers. In Stage IV, consistent levels of GAG are observed in the six-month-old native trachea, reflecting the mature state of cartilage (**Figure 2J-L**).

Chondrocyte protein expression during cartilage maturation: IHC assay: IHC staining revealed prominent expressions of key cartilage markers, including Sox9, aggrecan, type II collagen, and PCNA protein, in the early stages of neotissue development. A substantial number of chondrocytes strongly expressed these proteins in both the central and peripheral regions of the cartilage, highlighting active chondrogenic activity. At this stage, however, the perichondrium, a critical structural component for cartilage development, was absent from the edges of the growing cartilage (**Figure 3A-D**). As cartilage development progressed, the protein expressions profiles of chondrocytes began to diminish, particularly at the boundary regions of neocartilage. Although markers such as Sox9, aggrecan, and type II collagen remained positively stained in the central areas (**Figure 3E-H**). At this point, the perichondrium began to sprout along the edges of the growing cartilage, signaling the onset of its structural role in cartilage maturation. Over time, the overall expression levels of Sox9, aggrecan, and PCNA within the central cartilage regions continued to decline, reflecting reduced chondrocyte activity and proliferation. Nevertheless, protein residues and proliferative cells were still detectable within VCs, indicating their role in nutrient delivery and waste removal to support cartilage metabolism and development (**Figure 3I-L**). Ultimately, the process reached a stationary maturation phase. This stage was characterized by stabilized cartilage development, where the tissue exhibited features consistent with six-month-old native trachea (**Figure 3M-P**). Underscoring the dynamic nature of chondrogenesis and the critical roles of structural components like the perichondrium and VCs throughout the process (**Figure 2M**), significant differences were evident between the various stages of development (**Figure 3Q**).

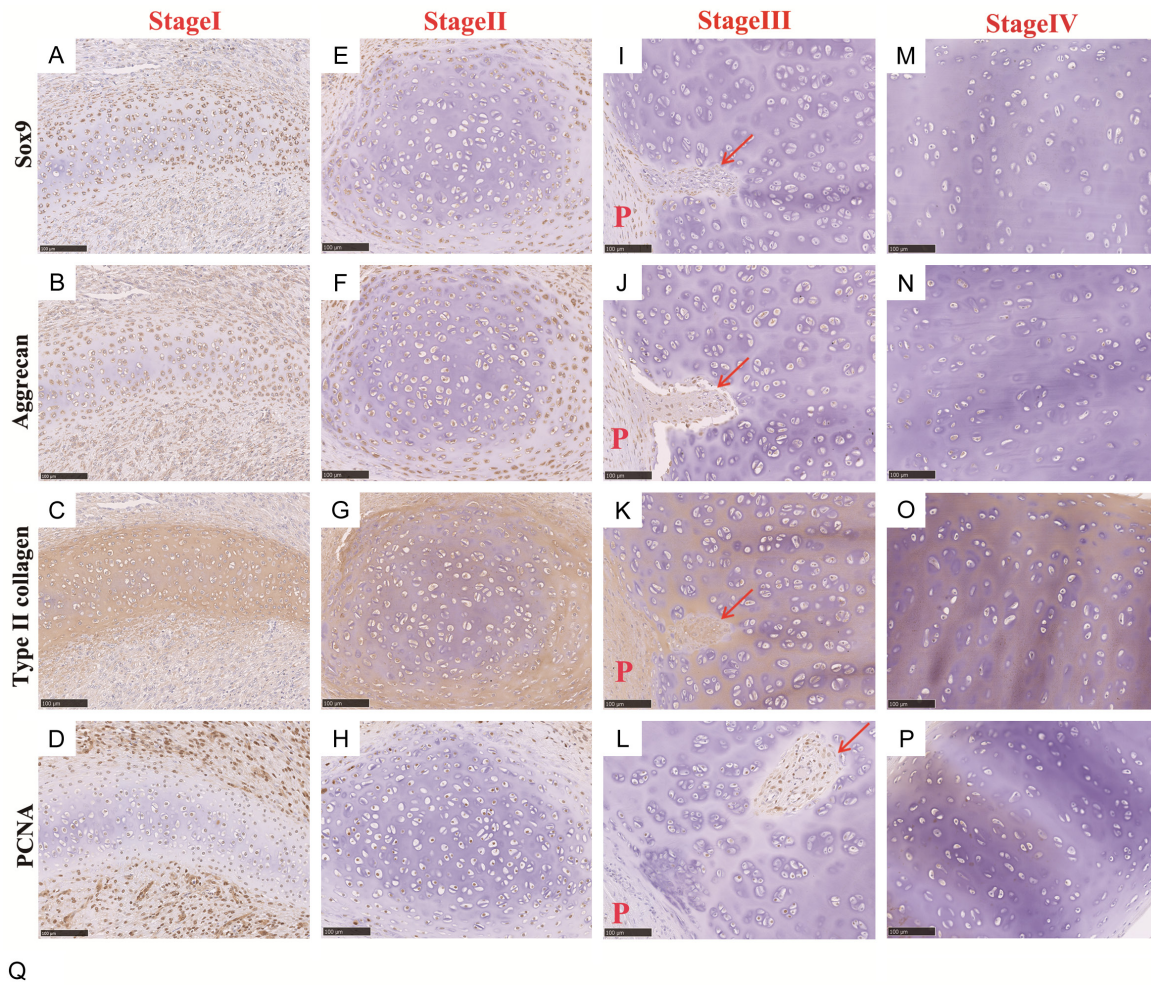
Interim PPs, PRLs, and VCs derived from perichondrium as chondro-modulators of cartilage maturation for pruning outnumbered chondrocytes in conjunction with degraded matrix emitted into VC, submucosa, and mucosa

The perichondrium, housing chondro-progenitor cells and chondroblasts, plays a crucial role in boosting chondrogenesis and elaborating interim chondro-modulators PP, PRL, and VC [12]. These modulators emerged from the perichondrium and migrated to the center of the cartilage for chondrolysis (**Figure S3B-D**). PPs, PRLs, and VCs derived from the perichondrium played a significant role in cartilage consolidation (**Figures 4** and **S5**). Neocartilage with numerous chondrocytes was auto-digested by corona-like VCs originating from the perichondrium. These VCs were involved in cartilage inclusion and corrosion (**Figure 5**). GAG debris from metabolism appeared in the adjacent mucosa and submucosa areas. Notably, the process of cartilage corrosion did not involve drainage through blood vessels but occurred via tissue diffusion into the glands of the mucosa and submucosa (**Figure 4C, 4E**). This was in contrast to the native vessels in these two areas where no such traces were found (**Figure 4D, 4F**). These findings suggested that the removal of matrix degradation during cartilage corrosion had occurred through tissue diffusion rather than through vascular drainage.

Proposed four-stage development of chondrogenesis in tracheal cartilage during regeneration

We proposed a tentative four-stage process to explain the evolving behavior of neocartilage based on the following criteria: (1) changes in the number and morphology of chondrocytes, along with variations in histologic patterns by H&E, alcian blue, and safranin O, as well as IHC results indicating expressions of distinct chondrocyte markers; (2) the involvement of chondro-modulators, including PP, PRL, and VC; and (3) the formation of the perichondrium. Our findings showed that the number of chondrocytes (mean \pm SD) was significantly higher in stage I than in other stages: stage I (173.25 ± 14.31), stage II (115.50 ± 7.55), stage III (53.75 ± 5.32), and stage IV (51.00 ± 1.41) (6-month-old native trachea) (**Figure 6A**). In the 3-month-old porcine model, more chondro-

3D-printed silicone grafts in animal model



Protein expression	Stage I (n=4)		Stage II (n=4)		Stage III (n=4)		Stage IV (n=4)		p value
	mean	±SD	mean	±SD	mean	±SD	mean	±SD	
Sox9 (%)	97.06	±0.59	66.40	±5.33	10.34	±2.38	16.15	±0.82	0.001**
Aggrecan (%)	97.19	±1.66	69.04	±7.85	65.02	±7.75	57.36	±7.72	0.018*
PCNA (%)	85.60	±7.49	45.71	±9.77	20.22	±7.10	13.73	±3.36	0.002**
Type II collagen	++++		++++		++++		++++		

Figure 3. Proposed stages of chondrogenesis within the graft neo-tissue using IHC (type II collagen, Sox9, aggrecan and PCNA antibodies) staining: Histology of the different stages of chondrogenesis was detected in IHC, using Sox9 (A, E, I, M), aggrecan (B, F, J, N), type II collagen (C, G, K, O), and PCNA (D, H, L, P) antibodies. Protein expressions of all markers were detected in brown reaction products. Red “P”: the perichondrium. Red arrows: the modulator structure of the perichondrial papillae (PP) in (I-K) or vascular canal (VC) in (L). Images were at 200x magnification. (Q) Quantitative analysis of protein expression levels and staining intensity across different stages of cartilage development. The data include the mean ± SD of protein expression for Sox9, Aggrecan, Type II Collagen, and PCNA, along with statistical comparisons (p values). Statistical significance is denoted by $P < 0.05$. Staining intensity is represented for type II collagen using a relative scale: + indicates weak staining; ++ indicates moderate staining; +++ indicates strong staining; ++++ indicates very strong staining.

cytes were present, but with smaller cell sizes compared with the 6-month-old native trachea (Figure S3C). The number of chondrocytes in the 3-month-old native trachea (N=8 in each group) was also significantly higher than in the 6-month-old porcine ($98.4 \pm 3.7 > 52.1 \pm 1.6$; $P <$

0.05) (Figure S3E). In terms of Sox9 expression, we found a declining trend with advancing stages (mean ± SD of stage I: 97.06 ± 0.59 , stage II: 66.40 ± 5.33 , stage III: 10.34 ± 2.38 , and stage IV: 16.15 ± 0.82) (Figure 6B). Interestingly, regarding the protein aggrecan, its

3D-printed silicone grafts in animal model

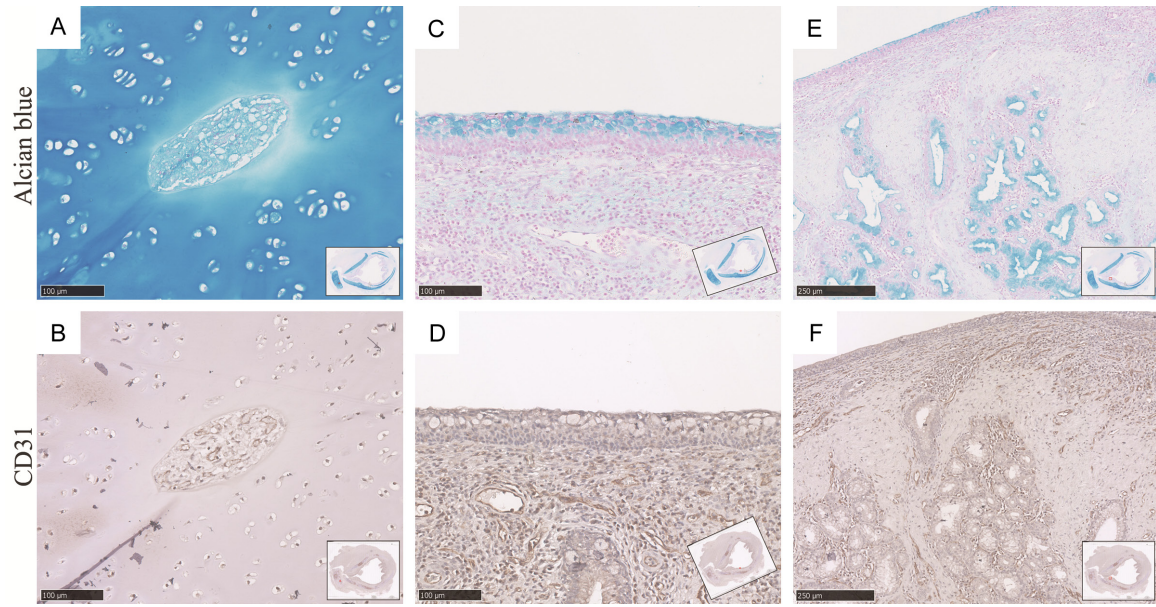


Figure 4. The matrix degradation product of cartilage was detected by alcian blue stain (A, C, E) and vessels were identified by reaction to CD31 antibody (B, D, F): Degradation product was detected in VCs (A) containing capillary vessels (B). The degradation matrix was identified within the stroma of the mucosa (C, D) and submucosal glands (E, F) of the trachea. (A-D): at 200× magnification; (E and F): at 100× magnification.

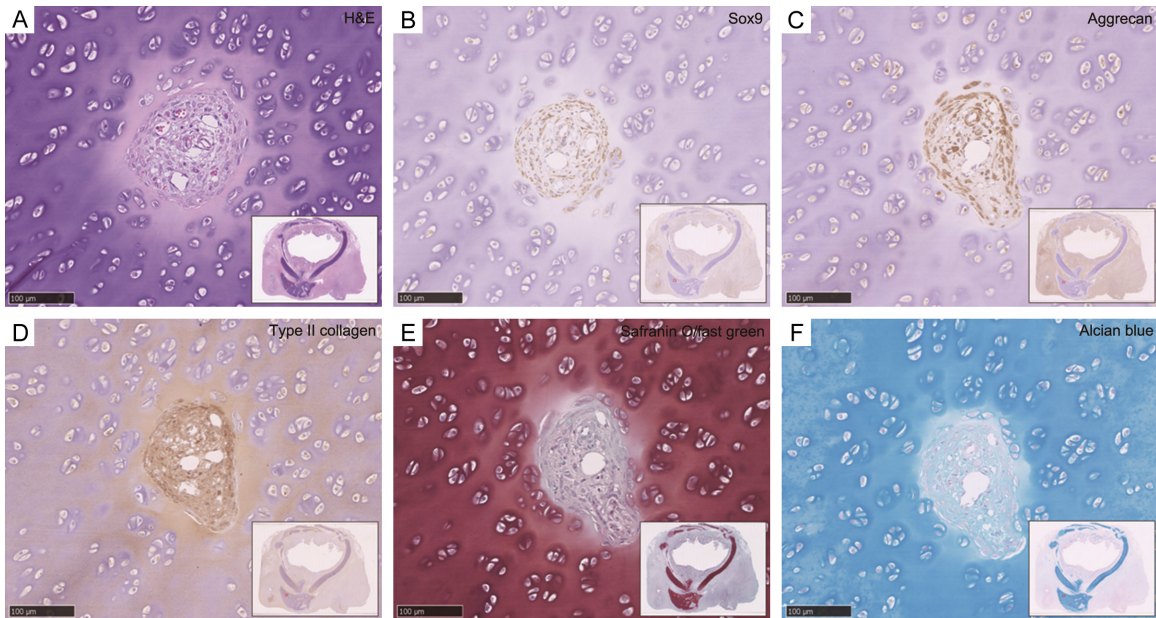


Figure 5. Characteristics of various staining of VCs in neocartilage, as detected by H&E, Sox9, aggrecan, type II collagen, safranin O/fast green and alcian blue: A. Histology showing results with H&E stain. B-D. Protein expressions as detected by Sox9, aggrecan, and type II collagen antibodies. E, F. GAG contents as shown with safranin O/fast green and alcian blue stain. Images are at 200× magnification.

chondrocyte expression was significantly higher in stage I than in other stages (II to V, all with similar expressions) (mean \pm SD of stage I: 97.19 ± 1.66 , stage II: 69.04 ± 7.85 , stage III: 65.02 ± 7.75 , and stage IV: 57.36 ± 7.72) (**Figure**

6C). Regarding proliferating cells (PCNA), we found more proliferating cells in the early stages with a gradual decline in the later stages (mean \pm SD of stage I: 85.60 ± 7.49 , stage II: 45.71 ± 9.77 , stage III: 20.22 ± 7.10 , and stage

3D-printed silicone grafts in animal model

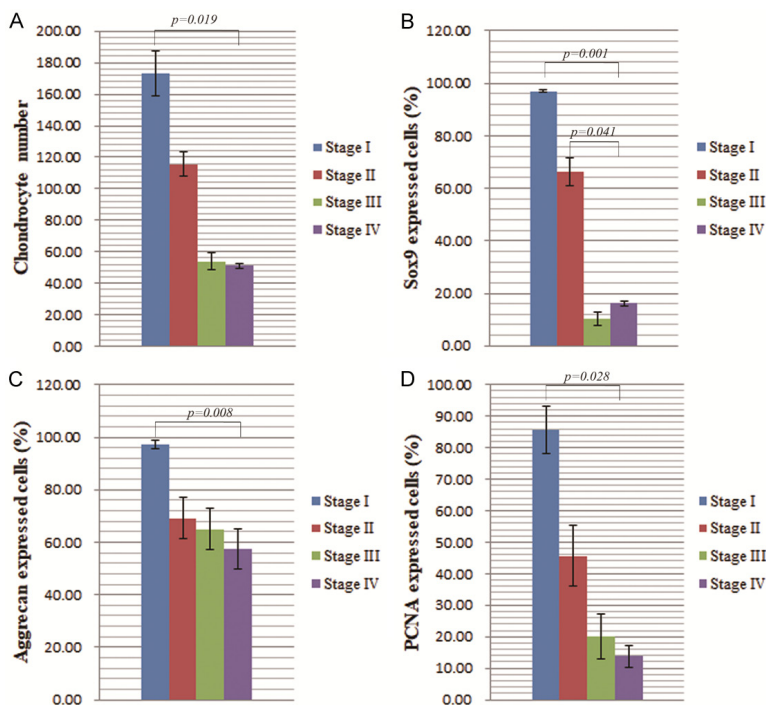


Figure 6. The data are shown as mean \pm SD and significant difference between the various stages ($P < 0.05$). Statistical analyses of the proposed stages of chondrogenesis within encasement of the graft neo-tissue based on H&E and IHC (Sox9, aggrecan, and PCNA antibodies) staining: (A) Chondrocyte numbers quantified for different stages of chondrogenesis of graft neo-tissue using the H&E stain ($n=4$ views at $400\times$ magnification for each group). (B-D) Ratios of protein expression (Sox9, aggrecan and PCNA) quantified for different stages of chondrogenesis of graft neo-tissue based on IHC staining ($n=4$ views at $200\times$ magnification for each group). Data are shown mean \pm SD values, and significant differences across various stages were set at $P < 0.05$.

IV: 13.73 ± 3.36) (**Figure 6D**). In brief, the highest number of chondrocytes and Sox9-, aggrecan-, and PCNA-positive cells appeared in stage I, when both the perichondrium and interim chondro-modulators (VC, PP, and PRL) were not present. Similar features were seen in stage II, which had a slightly reduced context but still lacked the perichondrium and modulators. Stage III showed little changes in chondrocyte number, Sox9-, aggrecan-, and PCNA-positive cells expressions compared with stage III, but was characterized by the presence of perichondrium and modulator structures. In stage IV, homeostasis in chondrogenesis was achieved with the presence of chondro-modulators (PP, PRL, and VC), in a condition similar to the six-month-old native trachea (**Figure S4E**).

Discussion

In this study, we uncovered a distinctive pattern of neotissue growth around the grafts, particu-

larly in cartilage. This growth was accompanied by concurrent developments in muscle, adipose tissue, and glands outside the 3D tracheal grafts in the three-month-old large-scale porcine model [15], typically occurring within approximately five days post-implantation (**Figure S2**). Using the proposed four-stage developmental framework, we systematically clarified the complex process of chondrogenesis during tracheal regeneration. This framework, supported by histologic staining techniques such as H&E, alcian blue, and safranin O, provided critical insight into the evolving behavior of neocartilage (**Figure 2**). Furthermore, IHC analysis revealed the expression of distinct chondrocyte markers (**Figure 3**). During the early phases, transitional chondrogenesis in neotissues was marked by a surge in growth, with numerous chondrocytes forming cartilage islands, paving the way for subsequent neocartilage development.

Following tracheal graft implantation, we observed two distinct cartilage growth patterns: (1) spear-like extensions of chondroblasts in certain areas, indicative of initial cartilage formation, and (2) the fusion of cartilage templates, signifying cartilage development progressing toward Stage III-IV. This variability highlights the complexity of cartilage regeneration within the neotissue [12, 17]. Recent reports have detailed the *de novo* generation of cartilage within grafts [18], corroborating our findings. Neocartilage development coincided with elevated levels of GAG and the appearance of chondro-modulators (PP, PRL, and VC), all originating from the perichondrium. The perichondrium, housing chondro-progenitor cells, plays a crucial role in boosting chondrogenesis [12, 19]. These chondro-modulators migrated to the cartilage center, influencing chondrolysis and consolidating cartilage by initiating the auto-digestion of neocartilage via corona-like VCs. Matrix degradation products from carti-

lage corrosion were detected in adjacent mucosa and submucosa areas (**Figure 3**), highlighting tissue diffusion rather than vascular drainage as the primary mechanism for matrix removal.

Chondrogenesis, angiogenesis, and adipogenesis were facilitated by the migration of mesenchymal stem cells (MSCs) to the graft site, enabling tissue regeneration [20]. Endogenous TGF- β , primarily produced by chondrocytes, stimulated chondrogenesis from MSCs sourced from peripheral blood and adipose tissue [21]. This process, akin to neurogenesis in the brain, involved periods of growth and consolidation regulated by neurotransmitters and neuromodulators. Tissue inflammation post-transplantation played a vital role, activating fibroblasts and regulating stem cells, which in turn drove chondrocyte differentiation and proliferation. As chondrogenesis progressed, chondrocytes formed discernible lacuna at the neocartilage periphery, while the perichondrium remained obscure. This was accompanied by strong GAG staining and increased protein expression in the cartilage's central region, reflecting the gradual accumulation of extracellular matrices. Specific stainings with safranin O and alcian blue delineated different stages of neocartilage formation, while VCs exhibited no safranin O staining, weaker alcian blue expression, and prominent type II collagen staining, indicating their role in cartilage degradation and maturation (**Figure 5**).

The perichondrium, acting as a reservoir of progenitor cells, differentiated into chondrocytes, enabling new extracellular matrix deposition and local colonization [22]. It also released cytokines supporting chondrogenesis. Key molecules such as BMP-2 [10, 23-26], Sox9 [27-29], and TGF- β 1 [10, 30] were instrumental in regulating cartilage growth and maturation by interactions with perichondrium progenitor cells during tracheal cartilage regeneration [31].

Chondro-modulators, VCs, PPs, and PRLs, critical to cartilage development, were discovered during *de novo* cartilage regeneration after 3D-printed tracheal grafting [12]. These modulators facilitated nutrient delivery and matrix degradation removal, which were vital for neocartilage metabolism. Vigorous angiogenesis in

the perichondrium of neocartilage, highlighted by CD31 enhancement, was more pronounced following tracheal transplantation compared to native tracheal cartilage [12]. PRLs and intravascular matrix degradation products indicated active cartilage corrosion, essential for metabolic and structural adaptation during regeneration [11].

Due to the absence of vasculature in tracheal cartilage, nutrient supply and waste removal often become compromised. VCs, PPs, and PRLs derived from the perichondrium, which contain vasculature, fulfilled these roles effectively [17], as evidenced by degradation products in mucosal and submucosal areas (**Figure 4**). Despite chondrogenesis, these degradation products indicated active cartilage corrosion, supporting tissue maturation. Coronary VCs facilitated this process by regulating autodigestion, evidenced by GAG debris in nearby blood vessels of the mucosa and submucosa.

The neocartilage exhibited varying staining patterns across different regions, leading to the proposal of a novel four-stage process to account for chondrogenesis in tracheal cartilage regeneration. Quantification of chondrocytes and positive cells expressing Sox9, aggrecan, and PCNA across these stages revealed significantly higher proliferative capacity during the initial stage than in later stages (**Figure 6**). Observations on changes in chondrocyte morphology and matrix contents provided a comprehensive understanding of cartilage evolution following graft implantation into the native trachea.

Limitations: Despite providing valuable insight into tracheal cartilage regeneration, results of our study are not suitable for immediate clinical translation. Further studies are needed for practical applications. The complex temporal dynamics of chondrogenesis, as outlined in our proposed four-stage framework, requires studies on individual or experimental variability.

In conclusion, 3D-printed tracheal grafts have enabled the *de novo* growth of cartilage with stent-sparing anastomoses. Our study provided a detailed exploration of chondrogenesis during tracheal regeneration. Results enhanced our understanding of the regenerative behavior as proposed by a four-stage chondrogenesis of tracheal neocartilage.

Acknowledgements

The authors sincerely appreciate the assistance provided by the Biostatistics Task Force, the Center for Translational Medicine, the 3-D Printing Research and Development Group, and the Department of Medical Research, Taichung Veterans General Hospital, Taichung, Taiwan. This research was funded by the Ministry of Science and Technology, Taiwan, Grant No. MOST 110-2314-B-075A-013-1; Taichung Veterans General Hospital and National Yang-Ming University, Taichung, Taiwan, Grant No. TCVGH-YM1100104; and Taichung Veterans General Hospital, Taichung, Taiwan, Grant No. TCVGH-1104701C.

Disclosure of conflict of interest

None.

Address correspondence to: Dr. Sen-Ei Shai, Division of Thoracic Surgery, Taichung Veterans General Hospital, 1650 Taiwan Boulevard Section 4, Taichung 40705, Taiwan. Tel: +886-4-2359-2525 Ext. 5050, +886-975-351-109; E-mail: sse50@yahoo.com; sse@vghtc.gov.tw

References

- [1] Lano CF Jr, Duncavage JA, Reinisch L, Ossoff RH, Courey MS and Netterville JL. Laryngotracheal reconstruction in the adult: a ten year experience. *Ann Otol Rhinol Laryngol* 1998; 107: 92-97.
- [2] Tan A, Cheng S, Cui P, Gao P, Luo J, Fang C and Zhao Z. Experimental study on an airway prosthesis made of a new metastable β -type titanium alloy. *J Thorac Cardiovasc Surg* 2011; 141: 888-894.
- [3] Kojima K, Bonassar LJ, Roy AK, Vacanti CA and Cortiella J. Autologous tissue-engineered trachea with sheep nasal chondrocytes. *J Thorac Cardiovasc Surg* 2002; 123: 1177-1184.
- [4] Shin YS, Choi JW, Park JK, Kim YS, Yang SS, Min BH and Kim CH. Tissue-engineered tracheal reconstruction using mesenchymal stem cells seeded on a porcine cartilage powder scaffold. *Ann Biomed Eng* 2015; 43: 1003-1013.
- [5] Tsukada H, Gangadharan S, Garland R, Herth F, DeCamp M and Ernst A. Tracheal replacement with a bioabsorbable scaffold in sheep. *Ann Thorac Surg* 2010; 90: 1793-1797.
- [6] Kim DY, Pyun J, Choi JW, Kim JH, Lee JS, Shin HA, Kim HJ, Lee HN, Min BH, Cha HE and Kim CH. Tissue-engineered allograft tracheal cartilage using fibrin/hyaluronan composite gel and its in vivo implantation. *Laryngoscope* 2010; 120: 30-38.
- [7] Kamil SH, Eavey RD, Vacanti MP, Vacanti CA and Hartnick CJ. Tissue-engineered cartilage as a graft source for laryngotracheal reconstruction: a pig model. *Arch Otolaryngol Head Neck Surg* 2004; 130: 1048-1051.
- [8] Duynstee ML, Verwoerd-Verhoef HL, Verwoerd CD and Van Osch GJ. The dual role of perichondrium in cartilage wound healing. *Plast Reconstr Surg* 2002; 110: 1073-1079.
- [9] Ozbek S, Kahveci R, Kahveci Z, Filiz G, Ozcan M and Sirmali S. Effect of lyophilized heterologous collagen on new cartilage formation from perichondrial flaps in rabbits: an experimental study. *Ann Plast Surg* 2003; 50: 528-534.
- [10] Chen H, Tan XN, Hu S, Liu RQ, Peng LH, Li YM and Wu P. Molecular mechanisms of chondrocyte proliferation and differentiation. *Front Cell Dev Biol* 2021; 9: 664168.
- [11] Gabner S, Häusler G and Böck P. Vascular canals in permanent hyaline cartilage: development, corrosion of nonmineralized cartilage matrix, and removal of matrix degradation products. *Anat Rec (Hoboken)* 2017; 300: 1067-1082.
- [12] Shai SE, Lai YL, Hung YW, Hsieh CW, Huang BJ, Su KC, Wang CH and Hung SC. De novo cartilage growth after implantation of a 3-D-printed tracheal graft in a porcine model. *Am J Transl Res* 2020; 12: 3728-3740.
- [13] Bhora FY, Lewis EE, Rehmani SS, Ayub A, Raad W, Al-Ayoubi AM and Lebovics RS. Circumferential three-dimensional-printed tracheal grafts: research model feasibility and early results. *Ann Thorac Surg* 2017; 104: 958-963.
- [14] Rehmani SS, Al-Ayoubi AM, Ayub A, Barsky M, Lewis E, Flores R, Lebovics R and Bhora FY. Three-dimensional-printed bioengineered tracheal grafts: preclinical results and potential for human use. *Ann Thorac Surg* 2017; 104: 998-1004.
- [15] Sen-Ei S. Primitive regenerated-tissue evolution in situ after implantation of a 3D-printed tracheal graft. *IJB* 2024; 5178.
- [16] Shai SE, Lai YL, Huang BJ, Yu KJ, Hsieh CW, Chen YS and Hung SC. Feasibility of in situ chondrogenesis for the entire umbilical cord in preliminary preparation for tracheal graft. *Am J Transl Res* 2021; 13: 1307-1321.
- [17] Shai SE, Lai YL, Hung YW, Hsieh CW, Su KC, Wang CH, Chao TH, Chiu YT, Wu CC and Hung SC. Long-term survival and regeneration following transplantation of 3D-printed biodegradable PCL tracheal grafts in large-scale porcine models. *Bioengineering (Basel)* 2024; 11: 832.
- [18] Martinod E, Paquet J, Dutau H, Radu DM, Bensidhoum M, Abad S, Uzunhan Y, Vicaut E

3D-printed silicone grafts in animal model

- and Petite H. In vivo tissue engineering of human airways. *Ann Thorac Surg* 2017; 103: 1631-1640.
- [19] Togo T, Utani A, Naitoh M, Ohta M, Tsuji Y, Morikawa N, Nakamura M and Suzuki S. Identification of cartilage progenitor cells in the adult ear perichondrium: utilization for cartilage reconstruction. *Lab Invest* 2006; 86: 445-457.
- [20] Baumann K. Stem cells: moving out of the niche. *Nat Rev Mol Cell Biol* 2014; 15: 79.
- [21] Chen MJ, Whiteley JP, Please CP, Ehlicke F, Waters SL and Byrne HM. Identifying chondrogenesis strategies for tissue engineering of articular cartilage. *J Tissue Eng* 2019; 10: 2041731419842431.
- [22] Zang M, Zhang Q, Davis G, Huang G, Jaffari M, Ríos CN, Gupta V, Yu P and Mathur AB. Perichondrium directed cartilage formation in silk fibroin and chitosan blend scaffolds for tracheal transplantation. *Acta Biomater* 2011; 7: 3422-3431.
- [23] Pang EK, Im SU, Kim CS, Choi SH, Chai JK, Kim CK, Han SB and Cho KS. Effect of recombinant human bone morphogenetic protein-4 dose on bone formation in a rat calvarial defect model. *J Periodontol* 2004; 75: 1364-1370.
- [24] Wright VJ, Peng H and Huard J. Muscle-based gene therapy and tissue engineering for the musculoskeletal system. *Drug Discov Today* 2001; 6: 728-733.
- [25] Kobayashi T, Lyons KM, McMahon AP and Kronenberg HM. BMP signaling stimulates cellular differentiation at multiple steps during cartilage development. *Proc Natl Acad Sci U S A* 2005; 102: 18023-18027.
- [26] Zhang L, Luo Q, Shu Y, Zeng Z, Huang B, Feng Y, Zhang B, Wang X, Lei Y, Ye Z, Zhao L, Cao D, Yang L, Chen X, Liu B, Wagstaff W, Reid RR, Luu HH, Haydon RC, Lee MJ, Wolf JM, Fu Z, He TC and Kang Q. Transcriptomic landscape regulated by the 14 types of bone morphogenetic proteins (BMPs) in lineage commitment and differentiation of mesenchymal stem cells (MSCs). *Genes Dis* 2019; 6: 258-275.
- [27] Liu CF, Samsa WE, Zhou G and Lefebvre V. Transcriptional control of chondrocyte specification and differentiation. *Semin Cell Dev Biol* 2017; 62: 34-49.
- [28] Zhao Q, Eberspaecher H, Lefebvre V and De Crombrugghe B. Parallel expression of Sox9 and Col2a1 in cells undergoing chondrogenesis. *Dev Dyn* 1997; 209: 377-386.
- [29] Akiyama H, Lyons JP, Mori-Akiyama Y, Yang X, Zhang R, Zhang Z, Deng JM, Taketo MM, Nakamura T, Behringer RR, McCrea PD and de Crombrugghe B. Interactions between Sox9 and beta-catenin control chondrocyte differentiation. *Genes Dev* 2004; 18: 1072-1087.
- [30] Wu M, Chen G and Li YP. TGF- β and BMP signaling in osteoblast, skeletal development, and bone formation, homeostasis and disease. *Bone Res* 2016; 4: 16009.
- [31] Yoon MH, Kim JH, Oak CH, Jang TW, Jung MH, Chun BK, Lee SJ and Heo JH. Tracheal cartilage regeneration by progenitor cells derived from the perichondrium. *Tissue Eng Regen Med* 2013; 10: 286-292.

3D-printed silicone grafts in animal model

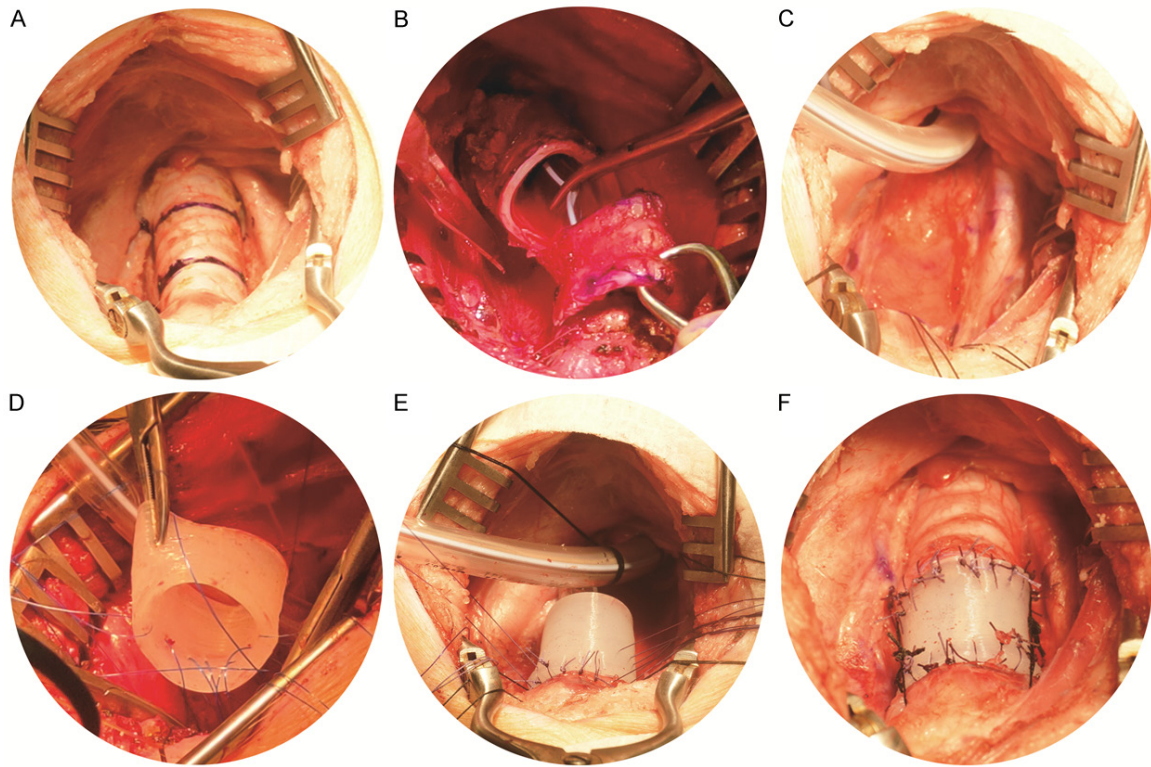


Figure S1. Procedures for surgical intervention for tracheal graft transplantation in a porcine model: A. Marking a two-cm long native trachea for resection. B, C. Removing the tracheal segment. C. Anastomosis at the proximal end of the trachea with graft. D, E. Completing the graft reconstruction. F. Graft reconstruction successfully completed.

Video S1. Procedures of surgical intervention of Silicone tracheal graft.

3D-printed silicone grafts in animal model

Table S1. Postoperative pharmacological management regimens for porcines undergoing tracheal graft transplantation

Drug administration time	Pharmacological agents	Dosing regimens	Administration procedures
4 hours post-operation	CEFAZOLIN SODIUM	2 g/Inj	Intramuscular (about 1.5 ml/pig)
4 hours post-operation	DEXAMETHASONE	5 mg/Inj	Intramuscular (about 0.5 ml/pig)
Note: After surgery, each pig received an intramuscular injection of one dose of antibiotics and steroids during the recovery period. The recovery room temperature was maintained at a suitable 25 °C, with a heat lamp provided to prevent a drop in the pig's body temperature. In cases of vomiting, any obstructions in the airway were cleared to ensure unobstructed breathing.			
Postoperative medication was administered continuously for 3 days	Voren-K	25 mg/capsule	Oral
Postoperative medication was administered continuously for 7 days	Prednisolone	5 mg/capsule	Oral
Postoperative medication was administered continuously for 7 days	Diflucan	50 mg/capsule	Oral
Postoperative medication was continuously administered until the animals were sacrificed	Curam	1000 mg/capsule	Oral
Postoperative medication was continuously administered until the animals were sacrificed	Bisolvon solution	20 mg/10 ml	Oral
Administered when the animal's wound infection was more severe	ENROTRIL CEFTIOFUR mixture	0.5 ml/10 kg 30-50 mg/10 kg	Intramuscular (about 1.5-2 ml/pig)

Note: During the postoperative observation period, the above-mentioned medications were administered once daily, either orally or via intramuscular injection. Additionally, cameras were installed in the animal housing room for 24-hour monitoring of the pigs' condition. The pigs' breathing, appetite, physical strength, and overall health status were observed at least twice a day.

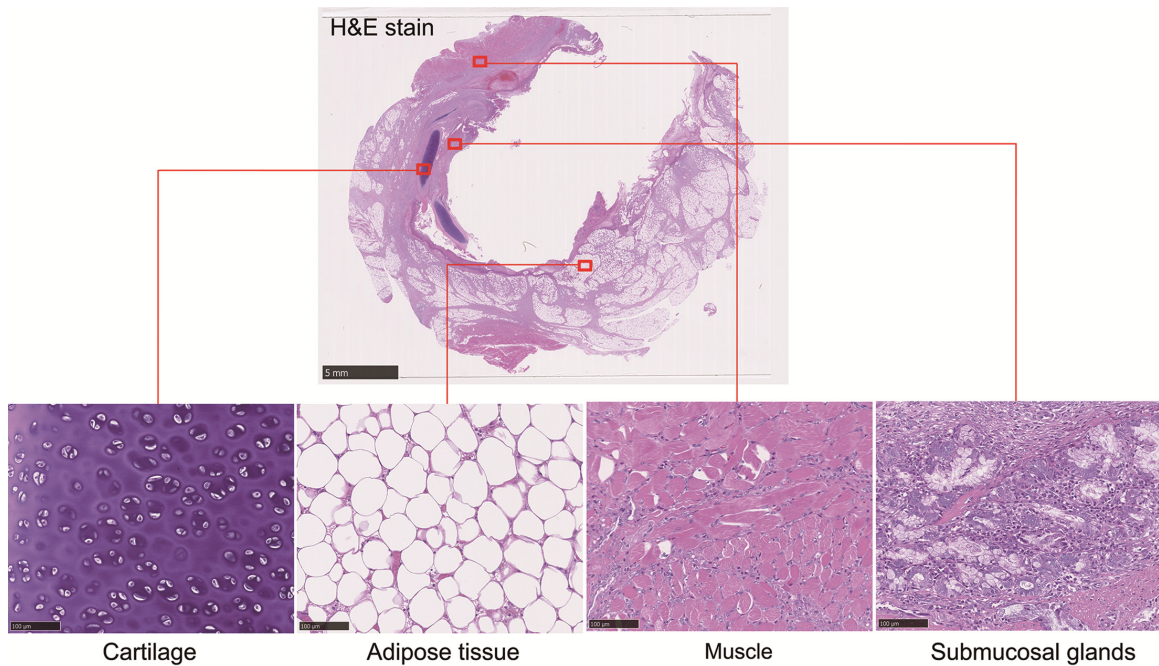


Figure S2. Vivid neo-tissue growth with cartilage, muscle, adipose and glands in areas outside the 3D-printed tracheal grafts after being transplanted into a three-month-old large-scale porcine model. Lower panel images magnified at 200 \times .

3D-printed silicone grafts in animal model

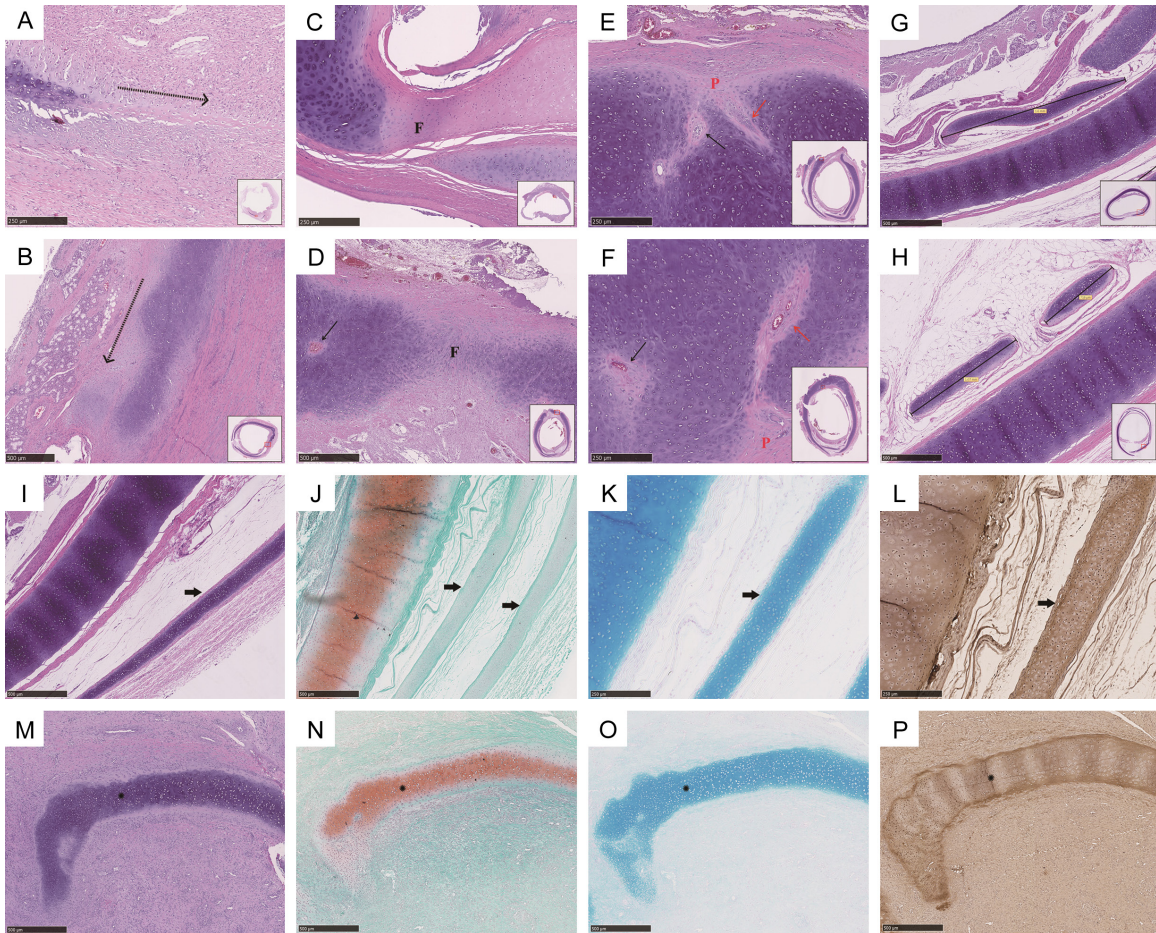


Figure S3. Neocartilage growth evolution in the form of either spear-like elongation or fusion at both ends of two neocartilages, showing chondro-modulators PP, PRL and VC within the neocartilages derived from perichondrium and porcine native trachea (A-H), as well as various stainings in three-month-old porcine native trachea and tracheal neocartilage (I-P): (A, B) Showing in the light area with H&E staining, the specific phenomenon of taper extension as discrete chondroblast infiltration through the blurred matrix (black dot arrow). (C, D) Neocartilage undergoing fusion during chondrogenesis under VC modulation: note its extension from regions of high-density chondrocytes in the perichondrium displaying clear lacuna within the dark area. The black “F” designates the fusion site of the neocartilage. (E, F) Showing presence of chondro-modulators PPs, PRLs and VCs within the neocartilage as derived from perichondrium. Black arrows: VCs; red arrows: PPs; and red “P”: perichondrium. (G) Showing a three-month-old porcine native trachea. (H) Showing a six-month-old porcine native trachea. Showing strong stainings to H&E, alcian blue and collagen II, and weak staining to safranin O in cartilage templates of native trachea. Black arrow: cartilage template. (M-P) Showing strong stainings to H&E, alcian blue and collagen II, and weak staining to safranin O in tracheal neocartilage. Black star: neocartilage. (A, C, E and F): at 100× magnification. (B, D, G-P): at 50× magnification.

3D-printed silicone grafts in animal model

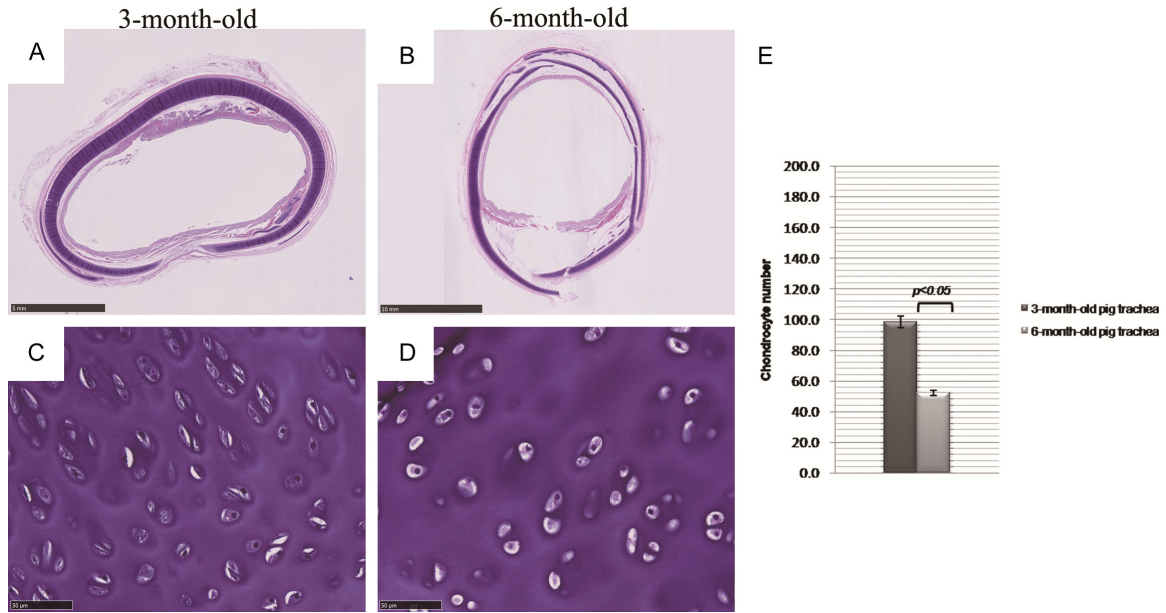


Figure S4. The shape of the tracheal lumen and chondrocyte morphology in the three- or six-month-old native porcine trachea: (A, C) three-month-old native porcine trachea. (B, D) Showing a six-month-old native porcine trachea. (E) Showing chondrocyte counts of three- and six-month-old native porcine tracheae ($n=8$ views of each group at 400 \times magnification, $P < 0.05$). Total views of histology in (A and B). (C and D) at 400 \times magnification.

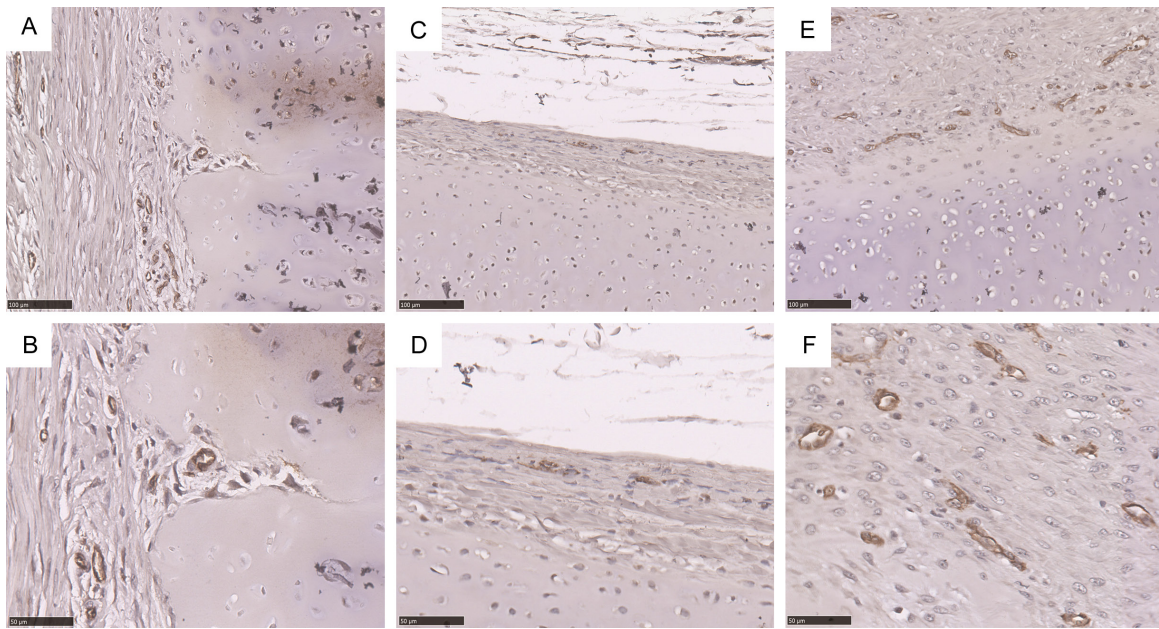


Figure S5. Capillaries in PPs and perichondrium were detected by reaction to CD31 antibody: (A, B) Capillary vessels in PPs. (C, D) Fewer capillary vessels identified within native three-month-old porcine trachea. (E, F) Abundant capillary vessels detected within tracheal neocartilage. (A, C and E) at 200 \times magnification; (B, D and F) at 400 \times magnification.